

## Letter

# State enhanced actinometry in the COST microplasma jet

David Steuer<sup>1,\*</sup> , Henrik van Impel<sup>1</sup> , Andrew R Gibson<sup>2</sup> ,  
Volker Schulz-von der Gathen<sup>3</sup> , Marc Böke<sup>3</sup>  and Judith Golda<sup>1</sup> 

<sup>1</sup> Plasma Interface Physics, Ruhr-University Bochum, D-44801 Bochum, Germany

<sup>2</sup> Research Group for Biomedical Plasma Technology, Ruhr-University Bochum, D-44801 Bochum, Germany

<sup>3</sup> Experimental Physics II: Physics of Reactive Plasmas, Ruhr-University Bochum, D-44801 Bochum, Germany

E-mail: [david.steuer@rub.de](mailto:david.steuer@rub.de)

Received 20 May 2022, revised 5 August 2022

Accepted for publication 9 September 2022

Published 30 September 2022



CrossMark

## Abstract

A new actinometry approach, helium state enhanced actinometry (SEA), is presented. This diagnostic uses the emission of the atomic states O( $3p^3P$ ) ( $\lambda = 844.6$  nm), Ar( $2p_1$ ) ( $\lambda = 750.4$  nm) and He( $3^3S$ ) ( $\lambda = 706.5$  nm) and allows the atomic oxygen density and the mean electron energy to be determined simultaneously from the spectral line intensity ratios. Here, the atomic states are selected in a way that they cover a wide range of the electron energy distribution function (EEDF). The method is compared to the classical actinometry approach and energy resolved actinometry (ERA) based on measurements on the COST microplasma jet. In addition, a benchmark against two-photon absorption laser induced fluorescence measurements is performed. Both atomic oxygen densities and mean electron energies are in good agreement with the literature. Furthermore, SEA offers a number of advantages over known approaches. Firstly, the experimental complexity is significantly reduced by using time-integrated spectra instead of phase-resolved measurements, as used in the original ERA approach. Secondly, the precision of the electron energy measurement can be significantly improved by the use of the helium state. In addition, known uncertainties e.g. due to excitation of oxygen excited levels via metastable oxygen states can be reduced.

Keywords: actinometry, optical emission spectroscopy, atomic oxygen, mean electron energy

(Some figures may appear in colour only in the online journal)

Reactive species such as atomic oxygen are needed for numerous applications including plasma medicine [1] or plasma catalysis [2]. To control and optimize these processes, it is

important to locally monitor the atomic oxygen densities. Typically this can be done using two-photon absorption laser induced fluorescence (TALIF) measurements [3]. However, this method has the disadvantage of requiring a complex laser system and non-trivial calibration. Furthermore, optical access for both laser beam and fluorescence signal must be available. This generally makes TALIF unsuitable for many setups, e.g. in industrial processes.

\* Author to whom any correspondence should be addressed.



Original content from this work may be used under the terms of the [Creative Commons Attribution 4.0 licence](https://creativecommons.org/licenses/by/4.0/). Any further distribution of this work must maintain attribution to the author(s) and the title of the work, journal citation and DOI.

An alternative diagnostic is optical emission spectroscopy. Quantification of atomic oxygen densities based on optical emission spectroscopy can be achieved by actinometry, which was originally introduced for silicon etch processes [4–7]. This method is characterized by its simplicity. Here, the atomic oxygen density is determined from the intensity ratio of two spectral lines. The observed atomic transitions belong to the species to be determined and to an actinometer gas of known density, typically argon. Here, the upper states are selected based on similar energy dependence and threshold of the electron impact excitation cross sections. Commonly used are the atomic oxygen state  $O(3p^3P)$  ( $\lambda = 844.6$  nm) and the argon state  $Ar(2p_1)$  ( $\lambda = 750.4$  nm). In the basic actinometry approach only direct electron impact excitation of the O and Ar states from the respective ground states are assumed to populate the excited levels, while processes such as dissociative electron impact excitation during electron collisions with molecules or excitation from metastables are neglected. Further assumptions and conditions for the actinometry approach which must be verified before the application of the diagnostic can be found in literature [6]. In general, these assumptions are only valid for a small range of plasma sources and operating conditions.

Previously, it has been shown that processes such as dissociative excitation of oxygen, can make a significant contribution to the population of excited states of atomic oxygen [6]. However, accounting for this contribution using the classical actinometry approach as Walkup *et al* [5] would require measurements of the shape of the electron energy distribution function (EEDF) and the mean electron energy, or at least model calculations as used by Katsch *et al* [6].

For this reason, a more advanced approach, energy-resolved actinometry (ERA), was introduced by Greb *et al* [8, 9]. This approach extends actinometry to include a third excited state of atomic oxygen  $O(3p^5P)$  ( $\lambda = 777.4$  nm). It applies the two-term approximation Boltzmann equation solver BOLSIG+ [10] to determine the shape of the EEDF and the corresponding rate coefficients for electron impact excitation of the corresponding excited states. The experimentally measured excitation ratios of the three spectral lines can be compared with the calculated values based on direct and dissociative electron impact excitation, allowing the mean electron energy as well as the atomic oxygen density to be determined. The method was benchmarked against TALIF measurements as well as numerical simulations, showing comparable results [8]. However, it is discussed in the literature that the additional oxygen state,  $O(3p^5P)$ , included in ERA can be populated via step-wise processes involving metastable oxygen atoms  $O(3s^5S^\circ \rightarrow 3p^5P)$  or molecules  $O_2(a^1\Delta_g)$  in addition to electron impact excitation and dissociative excitation from ground state atoms and molecules [6, 11]. Since these forms of excitation are not accounted for in the ERA calculations, the use of the emission at  $\lambda = 777.4$  nm can lead to uncertainties.

In this work, we present an alternative method, helium state enhanced actinometry (SEA). The atomic states used are chosen in a way that the excitation energies cover a wide range of the EEDF. By choosing the helium state  $He(3^3S)$

( $\lambda = 706.5$  nm) instead of the usual oxygen transition at 777.4 nm, the excitation energy increases from 10.7 eV to 22.7 eV, significantly widening the range of the EEDF that is probed. In addition, the method has two immediate advantages. Firstly, uncertainties due to the use of the emission at  $\lambda = 777.4$  nm and potential excitation via metastables can be reduced. Secondly, helium is used as a feed gas by default for a large number of plasma sources [12–14], allowing the emission to be measured without changing the plasma or admixing an additional gas.

In addition, the original ERA concept used the excitation ratios of each state, measured by phase resolved optical emission spectroscopy (PROES). Here, SEA is performed using time and space averaged emission intensity ratios. This simplification allows the application of the diagnostic for a wide range of plasma sources, since no spatially and temporally resolved ICCD setup is required, but a spectrometer is sufficient.

By measuring the three optical transitions, two emission intensity ratios can be formed:

$$\frac{I_{844}}{I_{750}} = c_1 \frac{f_{O_2} \nu_{844} a_{844} 2r_{O} k_{844,d}(\epsilon) + k_{844,de}(\epsilon)}{f_{Ar} \nu_{750} a_{750} k_{750,d}(\epsilon)} \quad (1)$$

$$\frac{I_{706}}{I_{750}} = c_2 \frac{f_{He} \nu_{706} a_{706} k_{706,d}(\epsilon)}{f_{Ar} \nu_{750} a_{750} k_{750,d}(\epsilon)}. \quad (2)$$

The emission of a transition depends on the fraction of the species in the total gas mixture  $f$ , the respective dissociation degree  $r_O = [O]/(2[O_2])$ , the photon energy  $h\nu_\lambda$  and the energy-dependent effective excitation rates  $k_\lambda(\epsilon)$  calculated by BOLSIG+ [10]. Factors  $c_1$  and  $c_2$  indicate calibration factors that compensate for the wavelength-dependent sensitivity of the setup. The indices d and de indicate direct electron impact excitation and dissociative excitation, respectively. Collisional quenching was considered for the optical branching ratio of the observed fluorescence transition ( $i \rightarrow k$ ):

$$a_\lambda = \frac{A_{ik}}{A_i + \sum_q k_q n_q}, \quad (3)$$

where  $A_{ik}$  is the Einstein coefficient for spontaneous emission,  $A_i$  the total spontaneous emission decay rate,  $k_q$  the quenching rate coefficient and  $n_q$  the absolute density of a quencher. Quenching rates for oxygen and argon can be found in the literature [15–17]. For the helium state, quenching rates by helium, argon and oxygen are unknown. However, it can be expected that the quenching by a molecular gas such as oxygen is significantly stronger than by atomic gases. Here, we assume that the quenching by molecular oxygen is of the order of molecular hydrogen, for which quenching rates are available [18]. In any case, for oxygen admixtures below 1% as considered in this work, collisional quenching does not modify the optical branching ratio significantly, although deviations should be considered for larger admixtures.

For these calculations, the cross section sets for He and  $O_2$  from the Biagi's Fortran code version 8.97, Magboltz database (LXCAT) [19] were used as input to BOLSIG+ [10]. In addition, the cross section for direct electron impact excitation

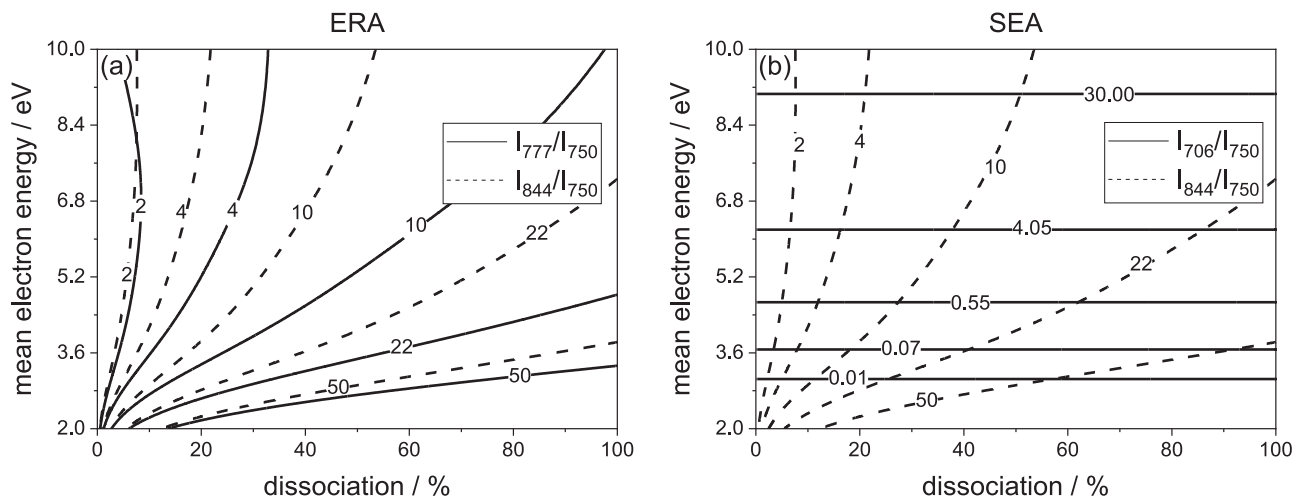


**Figure 1.** Exemplary calculated intensity ratios for (a) ERA:  $I_{777}/I_{750}$  and  $I_{844}/I_{750}$ , (b) SEA:  $I_{706}/I_{750}$  and  $I_{844}/I_{750}$  depending on the degree of dissociation  $r_O$  and the mean electron energy  $\epsilon$ . Numbers on the curves indicate the fixed intensity ratio. Conditions: 1 slm He, 5 sccm O<sub>2</sub>, 0.5 sccm Ar;  $T_{\text{gas}} = 350$  K.

of the Ar(2p<sub>1</sub>) state was taken from [20], while the cross sections for direct and dissociative excitation of the O(3p<sup>3</sup>P) and O(3p<sup>5</sup>P) states were taken from [21, 22], respectively. This combination of cross sections is chosen here for consistency with previous works on ERA [8, 9], and are also comparable with those used in other actinometry studies [11]. However, it should be noted that other cross sections are available in the literature and that a different combination of cross sections is likely to change the absolute densities and mean electron energies inferred from the actinometry calculations.

Figure 1 shows example solutions of the equations (1) and (2) as a function of the degree of dissociation and the mean electron energy. Each contour represents a fixed intensity ratio which can be measured. A solution of the equation system represents an intersection between two intensity ratios in figure 1. While figure 1(a) shows the ratios using the oxygen 777 nm line, figure 1(b) shows the ratios using the helium 706 nm line. Here, another advantage of SEA using the helium line becomes clear. The intensity ratio of helium and argon depends only on the mean electron energy but not on the dissociation degree. This leads to the fact that the contour lines in figure 1(b) intersect nearly perpendicularly. Using the oxygen line, however, the intensity ratios are nearly parallel under commonly used conditions for atmospheric pressure plasma jets (He + 0.5% O<sub>2</sub>), which makes it more complex to find unique solutions of the equation system [23].

In general, the use of time- and space-integrated emission intensities, which can be measured relatively easily, is a significant advantage over the use of time- and space-resolved measurements that are technically more challenging to implement. A major rationale behind the use of time- and space-resolved measurements in the original ERA approach [8, 9] is that temporal and spatial locations where the electron heating is strongest, and the fraction of excitation by single step electron impact processes (electron impact collisions with ground state atoms or molecules) is highest, can be selected and used in the actinometric calculations. In this way, states that can be

populated by step-wise processes can still be used, in principle. When time- and space-integrated measurements are used, the selection of excited states that are populated only single-step electron impact processes is even more important. Information on the relative importance of single step processes, that are strongly correlated with temporal and spatial regions of high electron heating, and step-wise processes involving metastable states, which are expected to be less modulated in time, can be obtained by comparing the temporal variation of the emission from each excited state.

Figure 2 shows the phase-resolved excitation into the different upper states. Here, the ‘COST Reference Microplasma Jet’ is used. This  $\mu$ -APPJ consists of two 30 mm long and 1 mm wide stainless steel electrodes to which a rf-voltage is applied. The discharge gap is 1 mm and enclosed in quartz panes. This well-defined plasma source is widely used due to its reproducibility [12, 24]. The measurements were acquired by an ICCD (Andor iStar DH334T-18U-73) equipped with a tunable filter (VariSpec NIR-RM-HC-20).

Typically, the excitation is given in two dimensional plots as a function of time and position between electrodes [25, 26]. In this work, the local dimension was integrated to compare the different states. Within one rf-period (13.56 MHz), there are two distinct periods of electron power absorption [25–27]. The states He(3<sup>3</sup>S), Ar(2p<sub>1</sub>) and O(3p<sup>3</sup>P) are highly modulated and almost not excited between the maxima. This indicates that single step electron impact processes dominate their formation and that their effective decay rates are on the same order. The state O(3p<sup>5</sup>P), on the other hand, is less modulated and is still populated between the maxima.

The lower modulation could, in principle, be explained either by stepwise excitation of the O(3p<sup>5</sup>P) state by metastable atoms or molecules or by lower collisional quenching. The latter can be excluded by comparing the collisional quenching rates constants with molecular oxygen as quenching partner ( $k_{\text{O}_2,777} = 10.8 \times 10^{-16} \text{ m}^3 \text{ s}^{-1}$  [15],  $k_{\text{O}_2,844} = 9.4 \times 10^{-16} \text{ m}^3 \text{ s}^{-1}$  [17]). It follows that the lower

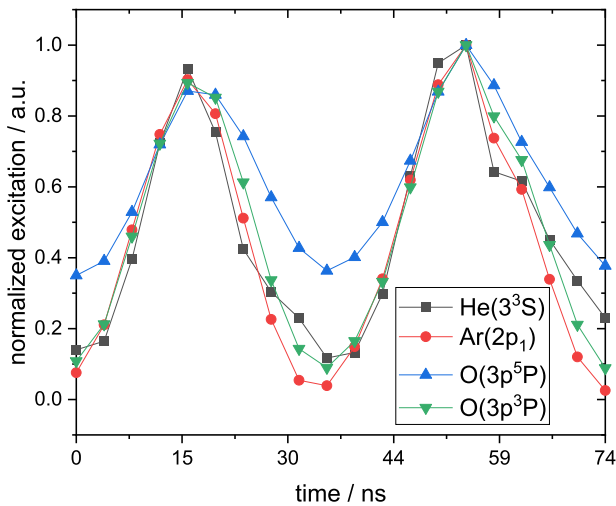


**Figure 2.** Phase resolved excitation into the states  $\text{He}(3^3\text{S})$ ,  $\text{Ar}(2p_1)$ ,  $\text{O}(3p^5\text{P})$  and  $\text{O}(3p^3\text{P})$ . Conditions: 1 slm He, 5 sccm  $\text{O}_2$ , 0.5 sccm Ar, 270 V,  $f = 13.56$  MHz.

modulation may be explained by an additional dissociative excitation channel for the formation of the  $\text{O}(3p^5\text{P})$  state via metastable molecules as suggested by Katsch *et al* [6], or stepwise excitation via metastable atoms as suggested by Caplinger *et al* [11]. The case for metastable atoms is supported by the much larger cross section for electron impact excitation of the metastable  $\text{O}(3s^5\text{S}^\circ) \rightarrow \text{O}(3p^5\text{P})$  (emission at 777 nm), when compared with electron impact excitation from  $\text{O}(3s^5\text{S}^\circ) \rightarrow \text{O}(3p^3\text{P})$  (emission at 844 nm), as reported by Barklem [28]. In addition, the lifetime of  $\text{O}(3s^5\text{S}^\circ)$  can be estimated under our conditions using the rate constants for collisional quenching given in [29] for He ( $1.8 \times 10^{-21} \text{ m}^3 \text{ s}^{-1}$ ) and  $\text{O}_2$  ( $2.2 \times 10^{-16} \text{ m}^3 \text{ s}^{-1}$ ). This is approximately 37 ns. Therefore, it can be concluded that  $\text{O}(3s^5\text{S}^\circ)$  can survive for a significant fraction of the radiofrequency period, during which it could contribute to stepwise excitation. From these simple arguments, it is plausible that step-wise excitation  $\text{O}(3s^5\text{S}^\circ)$  contributes to the emission at 777 nm under our conditions. However, to properly quantify the role of this process would require a more detailed model that also considers the density of this state.

The low modulation leads to the fact that time-resolved and time-integrated measurements differ strongly. In time-integrated measurements, the signals of the individual spectral lines are averaged over many rf periods and then the respective intensity ratios are formed. In time-resolved measurements, in contrast, it is possible to use only the signals at the time of the maximum intensity or excitation. In the case of the intensity ratio  $I_{777}/I_{750}$ , for the data shown in figure 2, the difference between time-resolved ratio (defined as the ratio between the absolute intensities at the time of maximum emission) and the time-integrated ratio (defined as the ratio between the absolute intensities averaged over one cycle) is 45%. Accordingly, when using the  $\text{O}(3p^5\text{P})$  state, a time-resolved measurement is required in order to use emission/excitation ratios at the time of maximum emission when an actinometry scheme that does not include step-wise excitation via metastable atoms and/or molecules is used. The remaining states, on the other

hand, are modulated in such a way that the deviation of excitation ratios due to time averaging is only 10%. In principle, this could make SEA also applicable for non-rf discharges, where PROES measurements are very complex. Nevertheless, it should be verified on a case-by-case basis whether these assumptions apply, for example, to other plasma sources or different gas compositions.

To qualify the SEA method, a benchmark against TALIF measurements is performed in the following. The setup used for TALIF, the performed calibration procedure and an estimate of the accuracy are described in detail in [30, 31]. For actinometry measurements a spectrometer (Avantes AvaSpecULS2048x64TEC-EVO 2011261U1) with an optical fiber (OceanOptics QP600-2-UV-BX) is used. The spectrometer has been relatively calibrated with a known light source (OceanOptics DH-3PLUS-BAL-CAL) and can resolve the spectral lines used to separate unwanted lines (0.3 nm resolution). To minimize uncertainties due to the low argon flows, a mass flow controller (Analyt) with a maximum flow of 1 sccm was used to precisely control small admixtures.

A comparative analysis between the classical actinometry approach, energy resolved actinometry, SEA and TALIF is shown in figure 3(a). The atomic oxygen density was determined in dependence of the applied driving voltage using the different methods. The confidence intervals of the actinometry approaches result from the size of the parameter range of dissociation degree and mean energy that are consistent with the solution of the system of equations. The accuracy of the TALIF measurements is based on the reproducibility of the data, as well as the noble gas calibration with xenon, which is described in more detail elsewhere [30]. Systematic errors that could affect the absolute densities, such as the choice of the two-photon excitation cross section ratio are not included in the confidence intervals [32].

The TALIF measurements show an approximately linear increase of the atomic oxygen density from 1 to  $3 \times 10^{21} \text{ m}^{-3}$  between 170 and 270 V. Both, the trend and the absolute value of the density are comparable to previous works [30, 31]. In contrast, the classical actinometry approach shows significantly higher densities (up to  $13 \times 10^{21} \text{ m}^{-3}$ ). This was expected, since the dissociative part of the excitation is not taken into account and therefore the density is overestimated.

Accounting for dissociative excitation is possible with ERA. The atomic oxygen densities range between 1 and  $3 \times 10^{21} \text{ m}^{-3}$ . In addition to atomic oxygen densities, ERA is also used to determine mean electron energies (see figure 3(b)). These are in the range between 13 and 15 eV, which is significantly higher than expected. However, as shown in figure 2, there is a significant deviation between the maximum and time integrated excitation of the  $\text{O}(3p^5\text{P})$  state and the other states used in ERA, potentially representing excitation via metastable atoms or molecules. Since such processes are not included in the ERA model, the use of ERA in this way may lead to a systematic error. This can also be illustrated by equations (1) or (2). Here, only excitation rates for single step electron impact excitation from the atomic ground state or dissociative excitation during collisions with  $\text{O}_2$  are used. If a significant part of the intensity comes from step-wise

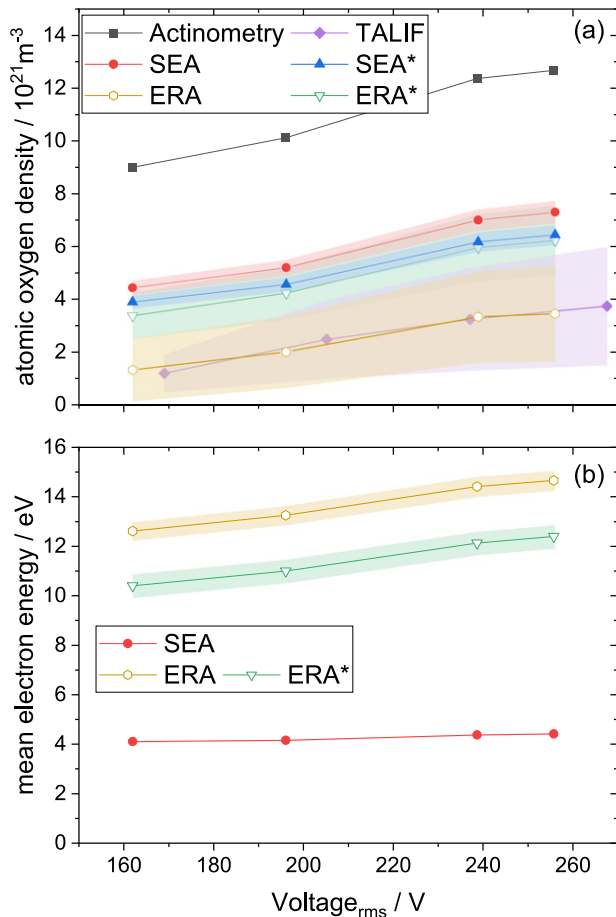


**Figure 3.** Atomic oxygen density (a) and mean electron energy (b) determined by various methods as a function of applied voltage. Colored areas: confidence intervals. Conditions: 1 slm He, 5 sccm O<sub>2</sub>, 0.5 sccm Ar.

excitation channels via metastables, this cannot be taken into account. Since the fraction of the excitation has to be compensated, it can be assumed that the mean energy is overestimated. If, the physical model underlying the ERA approach is incorrect when applied to temporally and spatially integrated spectra, as indicated by the artificially high mean electron energies, it can be assumed that the close agreement between ERA and TALIF measurements of atomic oxygen density is coincidental.

In an attempt to compensate for the difference between time-resolved and time-averaged measurements, the intensity ratios were modified. Here, a time-resolved measurement is evaluated and the ratio between the intensity ratios at the maximum and the time-averaged intensity ratios is determined. This results in a correction factor that compensates for the difference between time-resolved and time-averaged measurements. The results are denoted by ERA\* and give densities in the range of  $3$  to  $6 \times 10^{21} \text{ m}^{-3}$ . The mean electron energies are in the range between  $10$  and  $12 \text{ eV}$  and still significantly higher than expected.

By using the SEA method, issues related to the population of the O( $3p^5P$ ) via metastable levels can be avoided. Again, the intensity ratios were also corrected (SEA\*). However, since the

deviations between maximum excitation and integrated excitation are very small for the states used with SEA, the atomic oxygen density determined with and without a correction are very similar. The difference in the results from the corrected SEA\* and SEA is only 10% and the densities are in a range between  $4$  and  $7 \times 10^{21} \text{ m}^{-3}$ . For SEA the mean electron energies are lower ( $4.0$  to  $4.5 \text{ eV}$ ) than for ERA. No difference can be observed between SEA and SEA\*.

In literature, electron temperatures in the range between  $2$  and  $3 \text{ eV}$  are given for the COST microplasma jet [26, 33, 34] which are related to mean electron energies between  $3$  and  $5 \text{ eV}$  under the assumption of a Maxwell–Boltzmann distribution, thus there is a reasonable agreement with the SEA method. However, the energies differ significantly when ERA is used, although Greb *et al* [8] reported a good agreement ( $3$ – $6 \text{ eV}$ ) with this method in a comparable jet. The difference shows clearly that ERA is most reliable when performed with phase-resolved measurements, otherwise the influence of excitation via metastables and other processes is too large.

In addition to a difference in the absolute atomic oxygen density and mean electron energy, also a difference in the confidence intervals of ERA and SEA is noticeable. While the uncertainties for ERA are up to 90% (25% for ERA\*), for SEA uncertainties of around 5% are obtained. This difference results from the more clearly defined crossing points of the excitation ratios in the SEA scheme. This means that the ranges of dissociation degree and mean electron energy for which the experimentally measured ratios are consistent with the calculated ratios, are smaller. In addition, it becomes clear that the SEA method can access a larger energy range of the EEDF, which should allow it to provide a more robust estimate of the mean energy. Nevertheless, the confidence intervals indicate only the uncertainties of the calculation and not the systematic uncertainty caused by the numerous assumptions of actinometry.

Overall, the use of the SEA scheme together with time integrated spectra allows for a realistic estimation of both the atomic oxygen densities and mean electron energies. On the other hand, the use of ERA with time integrated spectra is capable of providing realistic estimations of atomic oxygen density under these specific conditions, but strongly overestimates the mean electron energy.

In summary, helium state-enhanced actinometry presented in this paper offers the possibility to determine atomic oxygen densities and mean electron energies simultaneously. SEA and TALIF measurements show good agreement for the atomic oxygen density in the COST microplasma jet and mean electron energies known from the literature could be reproduced. Known systematic errors in classical or energy-resolved actinometry can be reduced. The use of time-averaged emission makes only one spectrometer necessary. This significantly reduces the experimental complexity compared to laser diagnostics or phase-resolved spectroscopy measurements. Nevertheless, if a different plasma source is used, the systematic error due to time-integrated measurements should be experimentally verified. Furthermore, the helium line used can be observed in a large number of plasmas without the need to change the gas mixture. However, SEA can also be used in

plasma sources operated without helium by using a low helium admixture. This makes this diagnostic feasible for a larger number of applications in research and industry.




## Acknowledgments

The authors gratefully acknowledge fruitful discussions with Michael Mo from the University of York. This work is funded by Deutsche Forschungsgemeinschaft (DFG, German Research Foundation) within SFB 1316 (projects A6, B2 and B11).

## Data availability statement

The data generated and analysed during the current study are available at the following URI: <https://rdpcidat.rub.de/node/563>

## ORCID iDs

David Steuer  <https://orcid.org/0000-0003-3005-0829>  
 Henrik van Impel  <https://orcid.org/0000-0001-8283-0873>  
 Andrew R Gibson  <https://orcid.org/0000-0002-1082-4359>  
 Volker Schulz-von der Gathen  <https://orcid.org/0000-0002-7182-3253>  
 Marc Böke  <https://orcid.org/0000-0003-1062-5808>  
 Judith Golda  <https://orcid.org/0000-0003-2344-2146>

## References

- [1] Weltmann K D and von Woedtke T 2017 *Plasma Phys. Control. Fusion* **59** 014031
- [2] Bogaerts A *et al* 2020 *J. Phys. D: Appl. Phys.* **53** 443001
- [3] Niemi K, Schulz-von der Gathen V and Döbele H F 2001 *J. Phys. D: Appl. Phys.* **34** 2330–5
- [4] Coburn J W and Chen M 1980 *J. Appl. Phys.* **51** 3134–6
- [5] Walkup R E, Saenger K L and Selwyn G S 1986 *J. Chem. Phys.* **84** 2668–74
- [6] Katsch H M, Tewes A, Quandt E, Goehlich A, Kawetzki T and Döbele H F 2000 *J. Appl. Phys.* **88** 6232–8
- [7] Niemi K, Reuter S, Graham L M, Waskoenig J, Knake N, Schulz-von der Gathen V and Gans T 2010 *J. Phys. D: Appl. Phys.* **43** 124006
- [8] Greb A, Niemi K, O’Connell D and Gans T 2014 *Appl. Phys. Lett.* **105** 234105
- [9] Tsutsumi T, Greb A, Gibson A R, Hori M, O’Connell D and Gans T 2017 *J. Appl. Phys.* **121** 143301
- [10] Hagelaar G J M and Pitchford L C 2005 *Plasma Sources Sci. Technol.* **14** 722–33
- [11] Caplinger J E, Perram G P and Adams S F 2021 *Plasma Sources Sci. Technol.* **30** 015008
- [12] Golda J *et al* 2016 *J. Phys. D: Appl. Phys.* **49** 084003
- [13] Dzikowski S, Michaud R, Böttner H, Dussart R, Böke M and Schulz-von der Gathen V 2020 *Plasma Sources Sci. Technol.* **29** 035028
- [14] Douat C, Kacem I, Sadeghi N, Bauville G, Fleury M and Puech V 2016 *J. Phys. D: Appl. Phys.* **49** 285204
- [15] Dagdigan P J, Forch B E and Miziolek A W 1988 *Chem. Phys. Lett.* **148** 10
- [16] Sadeghi N, Setser D W, Francis A, Czarnetzki U and Döbele H F 2001 *J. Chem. Phys.* **115** 3144–54
- [17] Niemi K, Gathen V and Döbele H F 2005 *Plasma Sources Sci. Technol.* **14** 375–86
- [18] Gans T, Lin C C, Schulz-von der Gathen V and Döbele H F 2003 *Phys. Rev. A* **67** 012707
- [19] Biagi S F *Fortran code, Magboltz version 8.97* [www.lxcat.net/Biagi](http://www.lxcat.net/Biagi) (accessed 27 July 2021)
- [20] Chilton J E, Boffard J B, Schappe R S and Lin C C 1998 *Phys. Rev. A* **57** 267–77
- [21] Laher R R and Gilmore F R 1990 *J. Phys. Chem. Ref. Data* **19** 277–305
- [22] Schulman M B, Sharpton F A, Chung S, Lin C C and Anderson L W 1985 *Phys. Rev. A* **32** 2100–16
- [23] Mo M, Niemi K, Gibson A, Bowman C, O’Connell D and Gans T 2021 Atomic oxygen densities in pulsed inductively-coupled plasmas: laser spectroscopy & energy resolved actinometry *74th Annual Gaseous Electronics Conf. Bulletin of the American Physical Society vol 66* (American Physical Society) p 7 <https://meetings.aps.org/Meeting/GEC21/Session/GT51.3>
- [24] Riedel F *et al* 2020 *Plasma Sources Sci. Technol.* **29** 095018
- [25] Bischoff L *et al* 2018 *Plasma Sources Sci. Technol.* **27** 125009
- [26] Golda J, Held J and Schulz-von der Gathen V 2020 *Plasma Sources Sci. Technol.* **29** 025014
- [27] Gibson A R *et al* 2019 *Plasma Sources Sci. Technol.* **28** 01LT01
- [28] Barklem P S 2007 *Astron. Astrophys.* **462** 781–8
- [29] Mori T, Kanou K, Mizuta K, Kuramasu T, Ishikawa Y and Arai S 1992 *J. Chem. Phys.* **97** 9094–8
- [30] Korolov I, Steuer D, Bischoff L, Hübner G, Liu Y, Schulz-von der Gathen V, Böke M, Mussenbrock T and Schulze J 2021 *J. Phys. D: Appl. Phys.* **54** 125203
- [31] Steuer D, Korolov I, Chur S, Schulze J, Schulz-von der Gathen V, Golda J and Böke M 2021 *J. Phys. D: Appl. Phys.* **54** 355204
- [32] Drag C, Marmuse F and Blondel C 2021 *Plasma Sources Sci. Technol.* **30** 075026
- [33] Waskoenig J, Niemi K, Knake N, Graham L M, Reuter S, Schulz-von der Gathen V and Gans T 2010 *Plasma Sources Sci. Technol.* **19** 045018
- [34] Hemke T, Wollny A, Gebhardt M, Brinkmann R P and Mussenbrock T 2011 *J. Phys. D: Appl. Phys.* **44** 285206